XAS and XRF investigation of an actual HAWC glass fragment obtained from the Karlsruhe vitrification plant (VEK)

K. Dardenne [a], E. González-Robles [a], J. Rothe [a,*], N. Müller [a], G. Christill [b], D. Lemmer [c], R. Praetorius [c], B. Kienzler [a], V. Metz [a], G. Roth [a], H. Geckeis [a]

[a] Karlsruhe Institute of Technology, Institute for Nuclear Waste Disposal (KIT-INE), P.O. Box 3640, D-76021 Karlsruhe, Germany
[b] Karlsruhe Institute of Technology, Sicherheit und Umwelt (KIT-SUM), P.O. Box 3640, D-76021 Karlsruhe, Germany
[c] Wiederaufarbeitungsanlage Karlsruhe Rückbau- und Entsorgungs-GmbH, P.O. Box 1263, D-76339 Eggenstein-Leopoldshafen, Germany

A B S T R A C T

Several sections of HAWC glass rods remaining at the end of glass pouring at the Karlsruhe Vitrification Plant (VEK) were retained during vitrification operation in 2009 2010 and transferred to the KIT INE shielded box line for later glass product characterization. A mm sized fragment with a contact dose rate of ~590 μSv/h was selected for pilot XAS/XRF investigations at the INE Beamline for actinide science at the ANKA synchrotron radiation source. The experiment was aimed at elucidating the potential of direct radionuclide speciation with an emphasis on the fission products Se and Tc in highly active nuclear mate rials and at assessing the possible influence of the γ radiation field surrounding highly active samples on the beamline instrumentation. While the influence of γ radiation turned out to be negligible, initial radionuclide speciation studies by XAFS were most promising. In addition to Se and Tc speciation, the focus of these initial investigations was on the possibility for direct actinide speciation by recording cor responding L3 edge XAFS data. The registration of high quality XANES data was possible for the actinide elements U, Np, Pu and Am, as well as for Zr.

1. Introduction

The Karlsruhe Reprocessing Plant (“Wiederaufarbeitungsanlage Karlsruhe” WAK) was operated from 1971 to 1991 as a pilot facil ity for reprocessing of spent nuclear fuels. The plant had a capacity of reprocessing about 35 t heavy metal per year. In total around 200 t of spent nuclear fuel from German pilot reactors and com mercial power plants were processed. This reprocessing resulted in about 60 m^3 of highly radioactive waste concentrates (HAWC) stored in liquid form (i.e., nitric acid solution) in storage tanks. The solution had a total inventory of approximately 6×10^{17} Bq including all dissolved fission products, the minor actinides and $\leqslant$1 wt.% of the original uranium and plutonium masses. An impor tant step in the ongoing process of the WAK decommissioning and dismantling was the successful immobilization of the HAWC by vitrification. To this end, the Karlsruhe Vitrification Plant (“Ver glasungseinrichtung Karlsruhe” VEK) was constructed on site close to the HAWC storage facilities. The heart of the VEK, the pro cess technology, is based on the liquid fed ceramic lined waste glass melter (LFCM) which was developed by the Institute for Nuclear Waste Disposal (INE) of the Karlsruhe Institute of Technology (KIT) [1].

The LFCM technique is based on continuous liquid feeding of the HAWC into the melter. On top of the molten glass pool a cold cap is formed as reaction zone characterized by different layers. The top layer contains a pool of evaporating liquid. Below this lay er, the liquid is dried and the remaining constituents are subse quently calcined. In deeper regions the material (mainly oxides) undergoes melting reactions as it comes in contact with the premelted glass frit added as glass matrix. By convective processes, the waste oxides are mixed with and incorporated in the molten glass at temperatures of 1150 1200 °C. After sufficient retention time in the melter, the homogenized product is batch wise filled into steel canisters (glass coquilles) by a pouring system at the melter bottom. Details on the successful operation of the vitrifica tion facility VEK were presented in [2].

One specific characteristic of the LFCM technique is the Joule heating of the electrically conductive glass melt by an alternating current passing between submerged opposite electrodes in the melter. In order to get a well molten waste glass product and to guarantee smooth drainage of the product, a specific viscosity of the melt in the operating temperature range is required. Therefore, a base borosilicate glass was developed to meet the processing

* Corresponding author.
E-mail address: Joerg.Rothe@kit.edu (J. Rothe).

requirements after incorporation of the waste oxides and process chemicals [3]. The glass product was characterized with respect to its viscosity and specific electric resistivity, liquid liquid misci bility, crystallization tendency, waste loading capacity and chemi cal durability under repository conditions using inactive surrogates for fission products [4]. The vitrification process aimed at a 16 wt.% waste oxide loading in the final glass matrix. The resulting glass product composition is listed in Table 1 [5].

XAS (X ray Absorption Spectroscopy) studies of glass materials are numerously reported in the material sciences literature, cover ing such disparate applications as the investigation of historic arti facts (e.g., [6]) or geological specimen (e.g., [7]), characterization of optical glasses for solid state lasers (e.g., [8]) or the encapsulation of radiotoxic residues from nuclear fuel reprocessing (notably the work of McKeown et al. [9 16]). These studies benefit from the ability of X ray Absorption Fine Structure (XAFS) measurements to provide direct chemical speciation (e.g., determination of oxida tion states and coordination geometries) through analysis of the X ray Absorption Near Edge Structure (XANES) without the need for any sample pretreatment while the Extended X ray Absorption Fine Structure (EXAFS) reveals structural details on the local coor dination environments (bond lengths, neighboring atom types) of glass matrix constituents unlike standard X ray Diffraction (XRD) analysis, which is severely hampered by the amorphous nat ure of elemental networks in glassy materials lacking any long range order. Studies on glass materials have been systematically used by, e.g., the group of Fornasini and Dalba to demonstrate the strength of XAFS to reveal bonding properties like non Gaus sian pair distributions in disordered systems (cf. [17] and refer ences therein). XAFS studies have been focused both on network forming glass constituents (such as boron, e.g. [18] or silicon, e.g., [19]) and on various impurities or inclusions modifying the optical properties or the stability of the glass matrix under specific conditions.

Table 1
Target values of the glass product composition according to Grünewald et al., 2000 [5].

Fission product oxides	wt.% in the glass product	Actinides	wt.% in the glass product
SeO_2	0.02	UO_2	1.19
Rb_2O	0.06	Np_2O_3	0.09
SrO	0.17	PuO_2	0.04
Y_2O_3	0.13	Am_2O_3	0.08
ZrO_2	0.60	CmO_2	<0.01
MoO_3	0.93	*Corrosion products and process chemicals*	
TcO_2	0.24	Fe_2O_3	1.68
RuO_2	0.52	NiO	0.31
Rh_2O_3	0.13	CuO	<0.01
PdO	0.28	ZnO	<0.01
Ag_2O	0.02	PbO	<0.01
CdO	0.02	Na_2O	4.38
SnO_2	0.01	MgO	0.13
Sb_2O_3	<0.01	Al_2O_3	0.02
TeO_2	0.12	K_2O	0.05
Cs_2O	0.59	CaO	0.10
BaO	0.46	F	⩽0.01
La_2O_3	0.42	Cl	⩽0.01
CeO_2	0.65	P_2O_5	0.45
Pr_2O_3	0.29	Others	0.45
Nd_2O_3	1.04	*Glass components*	
Pm_2O_3	<0.01	SiO_2	50.40
Sm_2O_3	0.23	B_2O_3	14.78
Eu_2O_3	0.03	Al_2O_3	2.60
Gd_2O_3	0.08	Li_2O	2.94
		Na_2O	5.96
		CaO	4.45
		MgO	1.85
		TiO_2	1.01

Reports on the investigation of radioactive nuclear waste glass es by XAFS in the literature are generally sparse, reflecting the dif ficulties for investigations of even moderately radioactive samples at most synchrotron radiation laboratories. Most of these available studies are focused on the corrosion and leaching behavior of bor osilicate type waste glass simulates and the chemical behavior of fission product elements added (as mostly inactive isotopes) to mimic compositions and chemistry of real HAWC solutions. In one of the earliest studies dating from 1983 published in an early book on EXAFS and Near Edge Structure applications [20] Anto nini and coworkers report on the formation of metallic Tc clusters in a borosilicate glass doped with 2 wt.% ^{99}Tc. Greaves et al. [21] investigated the effect of water corrosion on the U L3 fluorescence EXAFS in surface sensitive grazing incidence detection mode (penetration depth about 3 nm) for a flat borosilicate glass wafer containing simulated nuclear waste with 3 wt.% cation concentra tion. Changes of the U L3 EXAFS signal of the corroded sample compared to the pristine surface are interpreted in terms of an U enrichment in the surface region and the corresponding increase of U U structural correlations. The chemical speciation of plutoni um in simulated sodalite/glass waste products was studied by Richmann et al. [22] by means of XAFS spectroscopy. They observed segregation of PuO_2(s) in the sodalite/glass matrix, yet it remained unclear whether Pu(IV) was kept within the sodalite lattice. Brendebach et al. [23] analyzed sulfur K edge XAFS spectra as part of a study aiming at borosilicate glass formulations capable to incorporate extended amounts of sulfur without the formation of an undesired separate "yellow phase", which exhibits less favor able leaching stability. XAFS and Raman spectroscopy studies on a candidate laboratory waste glass sample suggested that the sulfur is present in the glass as sulfate anion SO_4^{2-}, most probably as small Na_2SO_4 clusters in voids of the glass matrix. Using XAFS spec troscopy, Stefanovsky and Purans [24] analyzed the speciation of Cs in inactive sodium cesium borosilicate glasses. They observed that cesium ions occur in a slightly distorted twelve fold coordi nated oxygen environment at Cs_2O contents of 1 2 mol.%, whereas at higher Cs_2O contents the coordination number and average Cs—O bond distance decrease significantly. Researchers of the Catholic University of America, Washington DC, and the Glenn T. Seaborg Center at Lawrence Berkeley National Laboratory, Berke ley, CA, have put the dissimilar behavior of Tc and its chemical homolog Re in the same column of the periodic table into the focus on their spectroscopic studies on corroded borosilicate glasses [25 30]. Simulated waste glasses containing both Tc and Re were syn thesized under a variety of redox conditions to produce different distributions of Tc and Re oxidation states. These glasses were exposed to vapor hydration tests, followed by the determination of the Tc and Re oxidation state and coordination environment by Tc K /Re L2 XAFS and Raman spectroscopy. Compared with the original glasses, the corroded samples showed substantial reduction of Tc species, except where the original glass contained only reduced Tc (i.e., Tc^{4+}). Similar to earlier findings, Tc was more sensitive to redox conditions than Re with respect to both glass synthesis conditions and the following glass alteration process. Based on the results of their studies on corroded borosilicate glasses, these authors concluded that at least under the chosen conditions using Re as a non radioactive surrogate for Tc in borosilicate waste glasses can provide misleading results.

The present study summarizes initial results obtained from XAFS investigations of a fragment of borosilicate type HAWC glass molten during an industrial vitrification process with an emphasis on the fission products Se and Tc, which are regarded as contribut ing to the initially mobile fraction of the radionuclide inventory in spent nuclear fuel and waste glasses following corrosive waste degradation in a geological repository. To our knowledge, this is the first time ever that such a material has been transferred to

and analyzed at a synchrotron X ray beamline experimental sta tion. Note that XAFS measurements are performed on the actual HAWC actinide and fission product inventory generated during reactor fuel irradiation and not on mere surrogates.

2. Experimental

2.1. Sample preparation

During radioactive operation of the VEK vitrification plant, extending over a period of 9 months in 2009 2010, a total of 123 canisters were filled with about 48.8 metric tons of HAWC glass product. Centimeter sized sections of glass rods standing between the melter pouring system and the canister after solidification of the glass jet were retained during the filling of canisters #23 (0.437 g, dose rate 0.45 Sv/h), #57 (1.033 g, dose rate 0.50 Sv/h) and #71 (0.75 g, dose rate 0.50 Sv/h) and transferred to the INE shielded box line for later glass product characterization (cf. Fig. 1a). A mm sized rod fragment sampled from canister #57 (filled on January 21, 2010, at 2:00 am) with a mass less than 1 mg and a contact dose rate of 590 μSv/h was selected, removed from the shielded box in a contamination free vial and loaded into a specially designed container inside a ventilated fume hood at the INE controlled area laboratories. The sample container consists of a 8 mm thick Plexiglas disc with 30 mm diameter and a central cav ity of 2 mm diameter and 1 mm depth. After loading the container with the glass fragment, the cavity was covered by two crossed layers of self adhesive polyimide (Kapton®) tape of 25 μm thick ness. The dose rate in contact with the sample holder surface was ∼480 μSv/h. All surfaces were tested to be contamination free before enclosing the sample container by an additional polyethy lene bag (Fig. 1b). The sealed Plexiglas disc was mounted into a standard sample holder which was placed into a certified transport container for shipment to the synchrotron source.

An inactive borosilicate glass fragment molten during operation of the inactive prototype vitrification plant (“Pilotverglasungsan lage” PVA), employing the identical process technology devel oped at KIT INE (sample ID: PVA5_4, section D, canister filled in December 1999, with a well known composition of additives [4] simulating the actual HAWC chemistry), was analyzed as a refer ence sample at the beamline with the same detection scheme.

2.2. XAFS and XRF measurements

XAFS spectroscopy and semi quantitative X ray Fluorescence (XRF) analysis were performed at the INE Beamline for actinide science [31] at the synchrotron radiation source ANKA [32], KIT North Campus. Inside the beamline experimental hutch declared a temporary controlled area, the sample holder was removed from the transport container and placed on the sample positioning stage on the experimental table with the surface of the sample container at an angle of 45° relative to the impinging X ray beam. Note that, standing at the edge of the table at about 70 cm distance from the sample, the actual dose rate was diminished to ∼1.6 μSv/h. Coarse positioning of the glass fragment with the experimenter present inside the experimental hutch was guided by a green diode laser aligned to the X ray beam path. The precise alignment of the sam ple in the X ray beam was performed remotely controlled from outside the experimental hutch. The inactive reference glass was placed in front of the HAWC glass particle during sequential mea surements, keeping detection geometries for both samples as close as possible.

For recording XAFS and XRF spectra of the glass fragment, the standard fluorescence yield detection setup at the beamline was used, where the monochromatic radiation delivered by the Lemonnier type double crystal monochromator (DCM) equipped with a pair of Ge[422] crystals is focused by a toroidal mirror, delivering a beam spot size of ∼500 × 300 μm^2 at the sample posi tion at a photon energy of 18 keV. The intensity of the incoming beam (I_0) was monitored using an Ar filled ionization chamber at ambient pressure. A five pixel LEGe solid state detector (Canberra, Belgium) at an angle of 90° relative to the impinging beam and a distance of ∼110 mm from the sample was used for collecting X ray fluorescence radiation. The fluorescence signal emitted by the sample was analyzed by a digital X ray pulse processing sys tem (XIA DXP, Hayward, CA) to derive energy dispersive emission spectra and filtered element emission lines for all XAFS scans in fluorescence yield detection mode. XAFS spectra of energy calibra tion standards or concentrated reference samples were recorded in conventional transmission mode, either from metal foils or powder samples pressed into homogeneous boron nitride tablets, yielding an absorption edge jump of 0.5 1.

Due to the small size of the radioactive glass fragment, a precise mesh scan of 3 × 3 mm^2, 100 μm step size, was applied to localize the exact sample position. Owing to a slight mechanical instability of the DCM, leading to a drift of the monochromatic beam at the downstream sample position with the Bragg angle, this precise localization had to be repeated for excitation energies separated by several keV (e.g., at the Se K , the Zr K and the Tc K edges at 12.658, 17.998 and 21.044 keV, respectively (values indicating 1s binding energies of the corresponding metal species).

Semi quantitative analysis of energy dispersive XRF spectra (i.e., employing a multi channel analyzer or MCA) obtained for the HAWC glass fragment and the inactive PVA5_4 sample was performed by irradiating the samples with monochromatic syn chrotron radiation. MCA spectra were typically recorded for an integration time of 120 s and normalized to I_0 for quantitative comparison. The excitation energy was systematically varied (a) to efficiently excite selected elements above their absorption thresholds, (b) to reduce the effect of overlapping elemental lines and (c) to clarify the effect of the characteristic escape peaks [33] an artifact of the Ge solid state detector material, which interfer es with low lying sample element lines in the MCA spectra due to fluorescence energy partially transferred to an “escaping” Ge Kα,β photon (∼9.8 keV). XAFS scans at the Se, Zr, and Tc K and the U, Np, Pu and Am L3 absorption edges (corresponding $2p_{3/2}$ binding ener gies for metal species: 17.166, 17.610, 18.057 and 18.510 keV, respectively) were recorded in step by step mode with a step width of 0.5 eV in the XANES regions and equidistant k steps of 0.035 Å^{-1} in the EXAFS regions (where detection of extended spec tral ranges was adequate, considering element concentrations). Generally, I_0 was reduced to 70% peak intensity by detuning the DCM in the middle of a scan range and kept constant by a MOSTAB feedback system during XAFS data acquisition. Up to six scans were averaged to improve the signal quality. According to the glass composition in Table 1, Th was not expected to be present in the glass and, hence, was not detectable in XAFS scans across the Th L3 edge (16.3 keV). Only a very tiny absorption signature was detected by scanning the energy across the Cm L3 edge (18.97 keV). This signal was not sufficient to obtain useful XANES data in reasonable time. This finding fully agrees with the known composition of the HAWC oxide residue, where the Cm content is expected to reach about 1/10 of the Pu content, which, in turn, amounts to ∼1/30 of the U content of the HAWC glass.

Interpretation of XRF data was accomplished using the PyMCA Fluorescence Toolkit [34]. XAFS data analysis was based on stan dard procedures by normalizing energy calibrated XANES spectra to their edge jump and by fitting a model to EXAFS χ(k) data as implemented in the IFEFFIT [35] suit of programs, employing FEFF (v8.4, cf. [36] and references therein) derived scattering amplitude and phase functions.

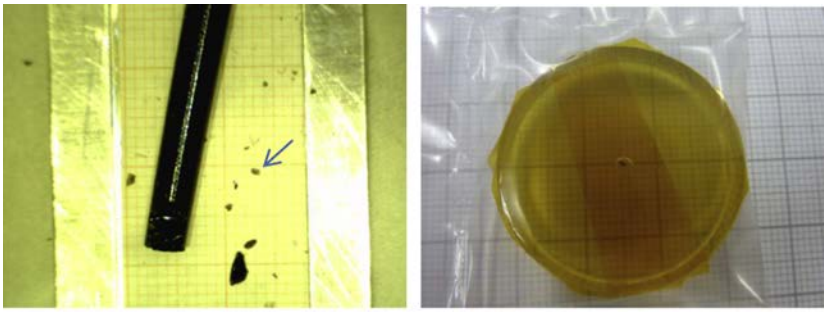

Fig. 1. (a) Photograph of glass rod section from canister #57 taken inside INE shielded box line – the particle used for the present study is marked by an arrow (scale in mm) and (b) HAWC glass fragment sealed in sample container.

3. Results and discussion

3.1. XRF analysis

Initial measurements were focused on the detection of possible effects of the γ radiation field surrounding the HAWC glass sample on the XRF data acquisition system at the beamline. Fig. 2 depicts a zoom into the overlain MCA spectra of the HAWC glass and the inactive reference sample PVA5_4, exhibiting the Fe, Ni and Zr K fluorescence lines (normalized to Ni Kα an Zr Kα intensity, respec tively). No differences in line shapes were observed for the selected element lines recorded for both the inactive and the radioactive HAWC sample. The presence of the radioactive sample did not visi bly increase the detector dead time. Thus, we hold effects of the persistent γ radiation background on the solid state detection and signal processing system during measurements of the HAWC glass at the given dose rate, isotope composition of the glass (the γ dose is dominated by the ^{137}Cs β$^-$ decay to ^{137m}Ba, which relaxes to ^{137}Ba through emission of 0.6617 MeV photons) and sample to detector distance to be negligible.

Fig. 3 shows an overview of the elemental X ray lines identified in the XRF spectra of the HAWC glass fragment, recorded for exci tation energies of 10.8, 14.5 and 21.5 keV. Fig. 4 depicts the corre sponding results obtained for the inactive PVA5_4 sample, where the highest excitation energy was set to 19.8 keV. To simplify qualitative comparison, the spectra recorded at 10.8 and 14.5 keV were scaled in both graphs by aligning the intensity of fluorescence

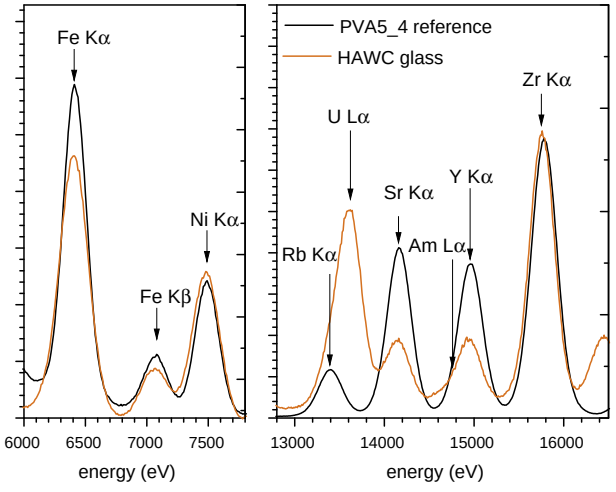

Fig. 2. Comparison of normalized MCA spectra in the region of Fe Kα,β, Ni Kα and Zr Kα lines obtained for the inactive reference sample and the HAWC glass fragment.

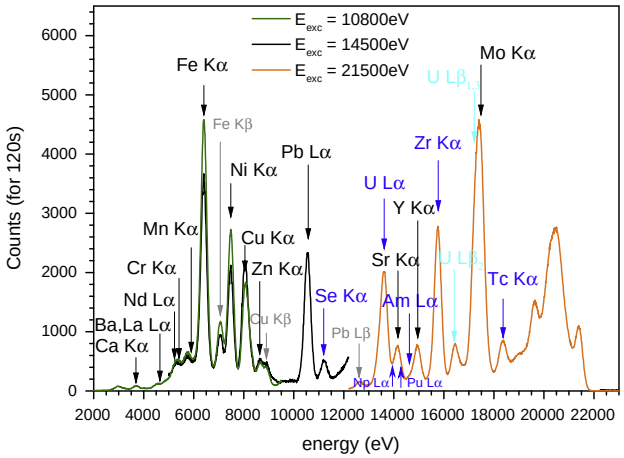

Fig. 3. XRF spectra taken from the HAWC glass fragment at different excitation energies and identification of some elements present in the sample. The elements investigated by XAFS spectroscopy in this study are marked in blue. (For interpretation of the references to color in this figure legend, the reader is referred to the web version of this article.)

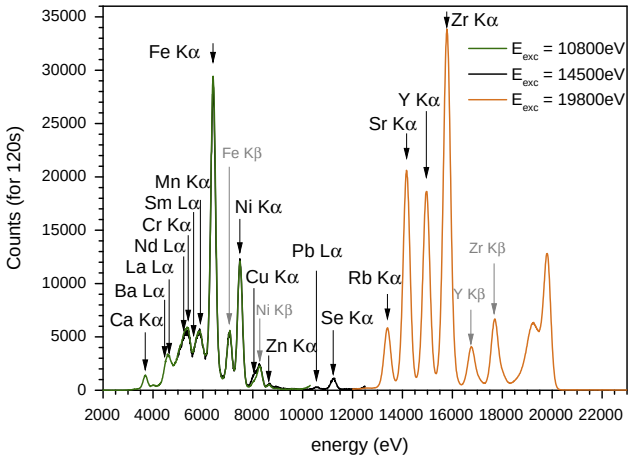

Fig. 4. XRF spectra taken from the inactive PVA5_4 reference glass at different excitation energies and identification of some elements present in the sample.

lines in the region between 4 and 8 keV. In addition to Se and Tc (cf. Section 1), clearly visible by their Kα emission lines, the plethora of elements originating from the vitrified HAWC feed solution is clearly detectable for the radioactive glass fragment including signals from the actinides U, Np, Pu and Am. Correspondingly,

the inactive surrogates added in case of the PVA5_4 reference glass show up in the MCA signals plotted in Fig. 4, where the actinides and Tc are absent. Due to inefficient excitation at high energies and strong (re)absorption of soft X ray photons below ~3.5 keV in the sample, the air between sample and detector and the detec tor windows, low Z elements are hard to detect with this experimental setup and, hence, have not been subject in the pre sent study. Elements marked in blue in Fig. 3 are selected for XAFS analysis and are discussed in more detail below.

Fig. 5 summarizes semi quantitative results in wt.% obtained by PyMCA analysis for selected elements present in the HAWC glass fragment compared to the waste glass target values calculated under the assumption of 16 wt.% oxide loading of the base borosi licate glass during the vitrification process (HAWC calc.). The val ues derived from emission line peak fitting are based on certain assumptions on the detection geometry, the known excitation energy and accumulated X ray photon dose, the absorbing effect of the air gap between sample and detector, the detector Be win dow and the sample containment, and the borosilicate base glass composition (according to Table 1) and density of 2.2 g/cm^3. How ever, as no certified standard was used, absolute values obtained for the HAWC glass sample by peak fitting deviate from the calcu lated target values by at least one order of magnitude. Neverthe less, good agreement for the relative abundance of different elements in the radioactive glass was achieved, as demonstrated in Fig. 5 by scaling the results from the measurement to the calcu lated results for Zr (HAWC exp.). Due to the high dose rate of the material, up to now no quantitative analysis of the HAWC glass produced during VEK operation by chemical digestion and, e.g., precise mass spectrometry has been attempted.

3.2. XAFS analysis

Initial radionuclide speciation studies of the HAWC glass frag ment by XAS were most promising. Fig. 6 depicts normalized Se K edge XANES measurements of the glass sample compared to spectra of selected Se reference samples. The spectrum of metallic Se(0) was as well recorded to calibrate the DCM energy scale by assigning the first inflection point in the rising absorption edge to the Se 1s binding energy (12658 eV), corresponding to the posi tion of the Fermi level. Fig. 7 shows the corresponding results obtained from the Tc K edge measurements. At the higher energy calibration was assured by measuring the Mo K edge of a Mo metal foil. Edge position and simple spectral fingerprint analysis unam biguously point to the presence of Se in the HAWC glass as selenite oxoanion (SeO_3^{2-}) as in the crystalline $Na_2Se(IV)O_3$ reference. The

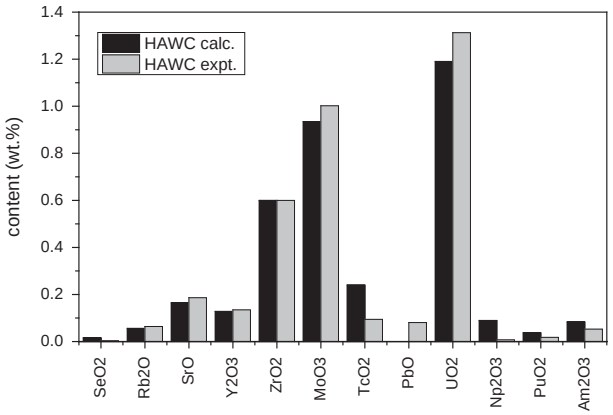

Fig. 5. Semi-quantitative analysis of the element content in the HAWC glass fragment using PyMCA software compared to the calculated values expected for a 16 wt.% oxide loading of the base borosilicate glass.

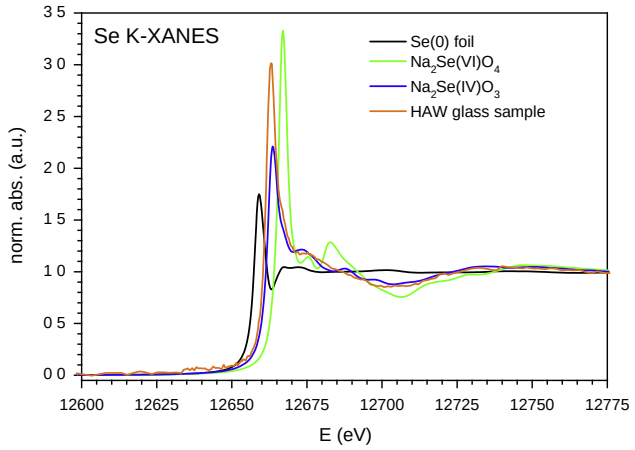

Fig. 6. Normalized Se K-XANES spectra of the HAWC glass fragment and corresponding reference spectra (cf. text for details).

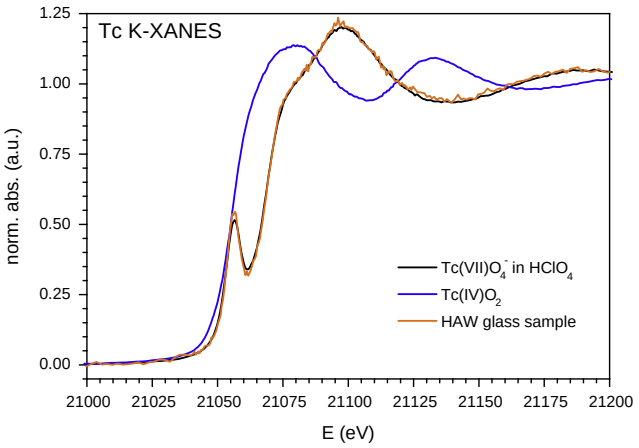

Fig. 7. Normalized Tc K-XANES spectra of the HAWC glass fragment and corresponding reference spectra (cf. text for details).

pronounced increase of the most intense spectral feature or "white line" (WL) at 12664 eV and the accompanying dampening of the fine structure above the edge observed for the HAWC sample indi cate dispersion of the SeO_3^{2-} entities in the glass matrix, where any crystalline ordering such as present in Na_2SeO_3 is lost. Tc is found dispersed as tetrahedral pertechnetate oxoanion (TcO_4^-) in the glass matrix as in the aqueous $Tc(VII)/HClO_4$ reference sample (apart from different noise levels, both spectra are congruent) unequivocally proven by the edge shift relative to $Tc(IV)O_2$ and the pronounced pre edge feature at ~21056 eV (a Tc 1s → 4d tran sition, indicative of tetrahedral oxygen coordination, lacking an inversion symmetry center as in $Tc(IV)O_2$).

Additional XAFS spectra of the HAWC glass sample were suc cessfully recorded for the actinides U, Np, Pu and Am at their L3 absorption edges, and for Zr at its K edge. The normalized XANES signatures are compared to corresponding reference spectra in Fig. 8 (U L3), Fig. 9 (Np L3), Fig. 10 (Zr K and Pu L3) and Fig. 11 (Am L3). Reference spectra for the crystalline actinide(IV) dioxides UO_2, NpO_2, PuO_2 and AmO_2 were obtained from [37 39], recorded in transmission mode at the same experimental station. Data for the Am(III) aqua ion was taken from [40] and displayed in Fig. 11 as reference for a trivalent Am species. The correctness of the ener gy scale (cf. the procedure indicated above) was assured by calibrating U and Np spectra vs. the K edge XANES of an Y metal foil (Y K edge energy at 17038 eV) and Pu, Zr and Am spectra vs.

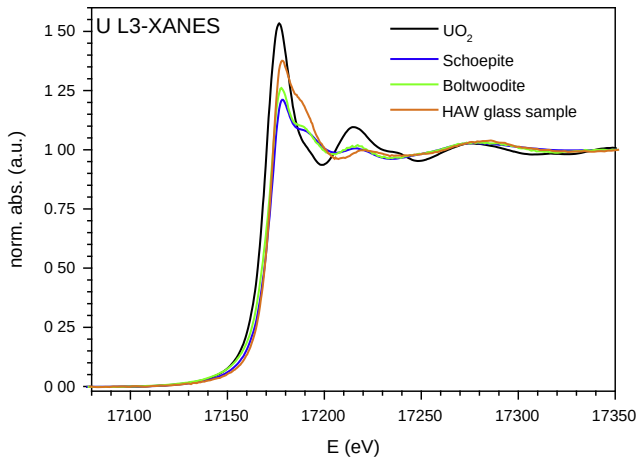

Fig. 8. Normalized U L3-XANES spectra of the HAWC glass fragment and corresponding reference spectra obtained for $U(IV)O_2$ and the uranyl minerals schoepite ($((U(VI)O_2)_8O_2(OH)_{12}\cdot 12(H_2O)$) and boltwoodite ($HK(U(VI)O_2)(SiO_4)\cdot 1.5(H_2O)$).

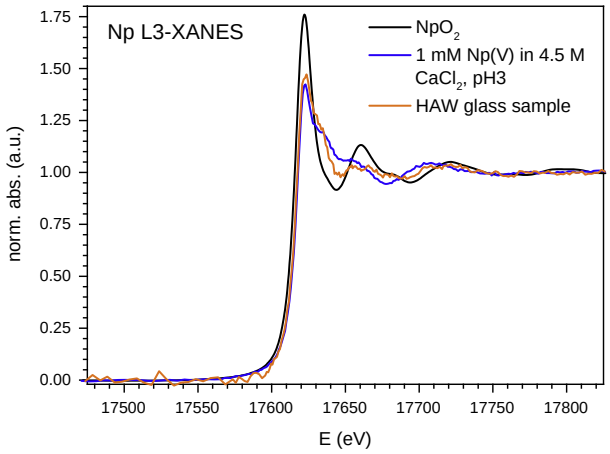

Fig. 9. Normalized Np L3-XANES spectra of the HAWC glass fragment and corresponding reference spectra obtained for $Np(IV)O_2$ and the Np(V) aqua ion.

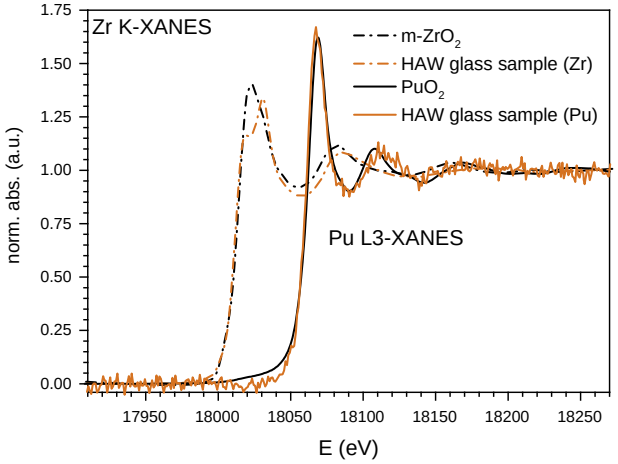

Fig. 10. Normalized Zr K- (dash-dotted lines) and Pu L3-XANES spectra (solid lines) of the HAWC glass fragment and corresponding reference spectra obtained for monoclinic $Zr(IV)O_2$ and $Pu(IV)O_2$.

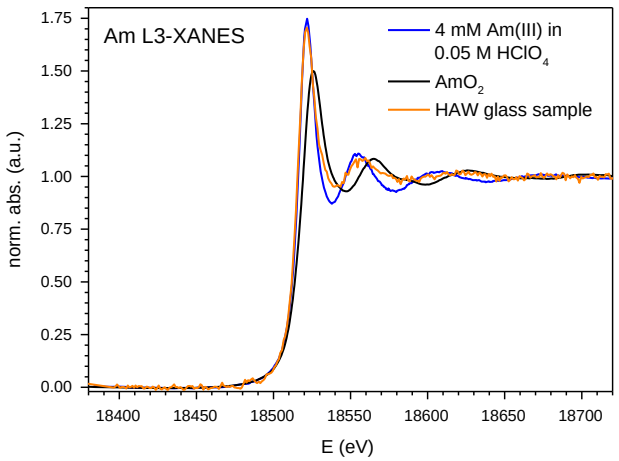

Fig. 11. Normalized Am L3-XANES spectra of the HAWC glass fragment and corresponding reference spectra obtained for $Am(IV)O_2$ and the Am(III) aqua ion.

the K edge XANES of a Zr metal foil (Zr K edge energy at 17998 eV), respectively. It is interesting to note that the scaling factors required to achieve the same edge jump of the normalized Np L3 (×16), Pu L3 (×24) and Am L3 XANES spectra (×10) as for the normalized U L3 spectrum rather well reflect the expected wt.% fractions of these elements at a 16 wt.% oxide loading of the glass: U 1.190%, Np 0.090%, Pu 0.037% and Am 0.083%. WL positions and characteristic actinyl (linear dioxo cations commonly formed by U, Np and Pu in their penta and hexavalent oxidation states) XANES features (i.e., the relatively low WL intensity and multiple scattering feature visible as a shoulder above the WL, cf., e.g., [41]) observed for U (E_{WL} = 17178.4 eV) and Np (E_{WL} = 17623.0 eV) unambiguously point to the presence of uranium as $(O{=}U(VI){=}O)^{2+}$ species and neptunium as $(O{=}Np(V){=}O)^{+}$ species in the HAWC glass (for comparison, e.g., [42]). Plutonium (E_{WL} = 18067.6 eV) and americium (E_{WL} = 18521.5 eV) are incorporated as tetra and trivalent Pu(IV) and Am(III) cations in the glass matrix, respectively. Zirconium, either originating from the fuel cladding or generated in the spent fuel as ^{235}U fission product, is present as tetravalent cation with a spectrum closely resembling that of the cubic zirconia polymorph c $Zr(IV)O_2$ [43] or that of octahedrally coordinated Zr(IV) in zektzerite ($LiNaZrSi_6O_{15}$) reported by McKeown et al. in their investigation of high zirconia borosilicate glasses [44]. This observation might indicate that Zr is incorporated into rather ordered local structures in the waste glass matrix in contrast to the fission products Se and Tc, where the corresponding XANES points to the disordered environment of the oxoanions.

4. Conclusions

It has been clearly demonstrated with the present study that direct determination of the speciation of possibly mobile fission products Se and Tc and the oxidation state of actinide elements U, Np, Pu and Am, present as minor constituents (below 1 wt.% with the exception of U) in a small fragment of radioactive HAWC glass, is possible without any sample pretreatment. Se was identified as selenite, Tc as pertechnetate, the actinides U, Np, Pu and Am are present in their hexa , penta , tetra and trivalent oxidation state as expected for the oxidative conditions during the VEK vitrification process [3]. The analysis of additional EXAFS data obtained in this study will be discussed in a forthcoming publication in comparison to data recently obtained for simulated HAWC reference glasses. XAFS investigation of additional elements like molybdenum or those belonging to the 3d elements and the lanthanide

series are possible and may be subject of a continuation of this pro ject. Determination of the relative abundance of some of the heav ier elements in the sample has been accomplished by semi quantitative XRF analysis (i.e., scaling the experimentally deter mined element contents in wt.% to the a priori known content of an element selected as internal standard). One open question aris ing at the beginning of this investigation was to the fate of iodine during the vitrification process. Due to its volatility at elevated temperatures, its high radiotoxicity and potential risk as bioavail able fission product, assessing the risk for the potential release of ^{128}I from a nuclear waste repository is of major concern. Unfortu nately, no unambiguous signal from iodine, which should show up by its most intense Lα fluorescence line at 3983 eV, was identified in our initial XRF measurements. We envisage the repetition of this investigation applying a low energy setup with a He atmosphere, more efficient excitation at the I L3 edge (4557 eV) and fluores cence detection by a silicon drift detector, thus avoiding the inter ference with detector based escape peaks.

To our knowledge, this is the first investigation of an actual HAWC glass sample from an industrial, radioactive vitrification process ever conducted at a synchrotron radiation beamline. The study also served as pilot experiment for ongoing investigations of spent nuclear fuel fragments at the INE Beamline at ANKA, employing the same sample containment concept and experimen tal procedures.

Acknowledgements

We thank E. Bohnert, W. Tobie and M. Plaschke (KIT INE) for helpful discussions. A. Bauer, Ch. Marquardt (both KIT INE) and Th. Hoffmann (KIT SUM) are acknowledged for invaluable techni cal and logistic support during preparation of these experiments. ANKA is acknowledged for the provision of beamtime.

References

[1] G. Roth, S. Weisenburger, Nucl. Eng. Des. 202 (2000) 197–207.
[2] M.W. F.J. Fleisch, G. Roth, W. Grünewald, W. Tobie, S. Weisenburger, Verglasungsanlage VEK – Erfolgreiche heiße Inbetriebsetzung und erste Betriebserfahrungen, in: Jahrestagung Kerntechnik, Berlin, Germany, 2010.
[3] B. Luckscheiter, M. Nesovic, Waste Manage. 16 (1996) 571–578.
[4] B. Luckscheiter, M. Nesovic, Waste Manage. 17 (1998) 429–436.
[5] W. Grünewald, G. Roth, W. Tobie, K. Weiß, Cold demonstration of the VEK vitrification technology in a full-scale mock-up facility, in: Waste Management WM'00 Conference, Tucson, Arizona, USA, 2000.
[6] R. Arletti, C. Giacobbe, S. Quartieri, G. Sabatino, G. Tigano, M. Triscari, G. Vezzalini, Archaeometry 52 (2010) 99–114.
[7] L. Wang, A. Yoshiasa, M. Okube, T. Hiratoko, Y. Hu, H. Arima, K. Sugiyama, J. Miner. Petrol Sci. 108 (2013) 288–294.
[8] T. Ohkura, Y. Fujimoto, M. Nakatsuka, J. Am. Ceram. Soc. 90 (2007) 3596–3600.
[9] D.A. McKeown, A.C. Buechele, H. Gan, I.L. Pegg, J. Non-Cryst. Solids 354 (2008) 3142–3151.
[10] D.A. McKeown, H. Gan, I.L. Pegg, J. Nucl. Mater. 420 (2012) 116–122.
[11] D.A. McKeown, H. Gan, I.L. Pegg, J. Non-Cryst. Solids 351 (2005) 3826–3833.
[12] D.A. McKeown, H. Gan, I.L. Pegg, W.C. Stolte, I.N. Demchenko, J. Nucl. Mater. 408 (2011) 236–245.
[13] D.A. McKeown, W.K. Kot, H. Gan, I.L. Pegg, J. Non-Cryst. Solids 328 (2003) 71–89.
[14] D.A. McKeown, I.S. Muller, H. Gan, Z. Feng, C. Viragh, I.L. Pegg, J. Non-Cryst. Solids 357 (2011) 2735–2743.
[15] D.A. McKeown, I.S. Muller, H. Gan, I.L. Pegg, C.A. Kendziora, J. Non-Cryst. Solids 288 (2001) 191–199.
[16] D.A. McKeown, I.S. Muller, H. Gan, I.L. Pegg, W.C. Stolte, J. Non-Cryst. Solids 333 (2004) 74–84.
[17] A. Kuzmin, G. Dalba, P. Fornasini, F. Rocca, O. Sipr, Phys. Rev. B 73 (2006).
[18] B. Cochain, D.R. Neuville, G.S. Henderson, C.A. McCammon, O. Pinet, P. Richet, J. Am. Ceram. Soc. 95 (2012) 962–971.
[19] G.S. Henderson, J. Non-Cryst. Solids 183 (1995) 43–50.
[20] M. Antonini, C. Caprile, A. Merlini, J. Petiau, F.R. Thornley, EXAFS and XANES investigation of the coordination of technetium in borosilicate glass, in: A. Bianconi, L. Incoccia, S. Stipcich (Eds.), EXAFS and Near Edge Structure, Springer, Berlin Heidelberg, 1983, pp. 261–264.
[21] G.N. Greaves, N.T. Barrett, G.M. Antonini, F.R. Thornley, B.T.M. Willis, A. Steel, J. Am. Chem. Soc. 111 (1989) 4313–4324.
[22] M.K. Richmann, D.T. Reed, A.J. Kropf, S.B. Aase, M.A. Lewis, J. Nucl. Mater. 297 (2001) 303–312.
[23] B. Brendebach, M.A. Denecke, G. Roth, S. Weisenburger, J. Phys. Conf. Ser. 190 (2009).
[24] S.V. Stefanovsky, J.J. Purans, Phys. Chem. Glasses B 53 (2012) 186–190.
[25] A.C. Buechele, D.A. McKeown, W.W. Lukens, D.K. Shuh, I.L. Pegg, J. Nucl. Mater. 429 (2012) 159–165.
[26] W.W. Lukens, D.A. McKeown, A.C. Buechele, I.S. Mueller, D.K. Shuh, I.L. Pegg, Abstr. Pap. Am. Chem. S. 234 (2007).
[27] W.W. Lukens, D.A. McKeown, A.C. Buechele, I.S. Muller, D.K. Shuh, I.L. Pegg, Chem. Mater. 19 (2007) 559–566.
[28] D.A. McKeown, A.C. Buechele, W.W. Lukens, D.K. Shuh, I.L. Pegg, Environ. Sci. Technol. 41 (2007) 431–436.
[29] D.A. McKeown, A.C. Buechele, W.W. Lukens, D.K. Shuh, I.L. Pegg, Radiochim. Acta 95 (2007) 275–280.
[30] D.A. McKeown, A.C. Buechele, C. Viragh, I.L. Pegg, J. Nucl. Mater. 399 (2010) 13–25.
[31] J. Rothe, S. Butorin, K. Dardenne, M.A. Denecke, B. Kienzler, M. Loble, V. Metz, A. Seibert, M. Steppert, T. Vitova, C. Walther, H. Geckeis, Rev. Sci. Instrum. 83 (2012).
[32] ANKA Light Source. <www.anka.kit.edu>.
[33] R. Durak, Y. Özdemir, Instrum. Sci. Technol. 29 (2001) 185–192.
[34] V.A. Solé, E. Papillon, M. Cotte, P. Walter, J. Susini, Spectrochim. Acta Part B 62 (2007) 63–68.
[35] B. Ravel, M. Newville, J. Synchrotron Radiat. 12 (2005) 537–541.
[36] A.L. Ankudinov, J.J. Rehr, J. Synchrotron Radiat. 10 (2003) 366–368.
[37] R. Böhler, M.J. Welland, D. Prieur, P. Cakir, T. Vitova, T. Pruessmann, I. Pidchenko, C. Hennig, C. Guéneau, R.J.M. Konings, D. Manara, J. Nucl. Mater. 448 (2014) 330–339.
[38] U. Carvajal-Nunez, D. Prieur, T. Vitova, J. Somers, Inorg. Chem. 51 (2012) 11762–11768.
[39] D. Prieur, J.-F. Vigier, T. Wiss, A. Janssen, J. Rothe, A. Cambriani, J. Somers, J. Solid State Chem. 212 (2014) 7–12.
[40] S. Stumpf, T. Stumpf, K. Dardenne, C. Hennig, H. Foerstendorf, R. Klenze, T. Fanghanel, Environ. Sci. Technol. 40 (2006) 3522–3528.
[41] M.A. Denecke, Coordin. Chem. Rev. 250 (2006) 730–754.
[42] B. Brendebach, N.L. Banik, C.M. Marquardt, J. Rothe, M.A. Denecke, H. Geckeis, Radiochim. Acta 97 (2009) 701–708.
[43] P. Li, I.W. Chen, J.E. Penner-Hahn, Phys. Rev. B 48 (1993) 10063–10073.
[44] D.A. McKeown, I.S. Muller, A.C. Buechele, I.L. Pegg, J. Non-Cryst. Solids 258 (1999) 98–109.

Karlsruher Institut für Technologie

OPEN ACCESS

Repository KITopen

Dies ist ein Postprint/begutachtetes Manuskript.

Empfohlene Zitierung:

Dardenne, K.; Gonzalez-Robles, E.; Rothe, J.; Müller, N.; Christill, G.; Lemmer, D.; Praetorius, R.; Kienzler, B.; Metz, V.; Roth, G.; Geckeis, H.
XAS nd XRF investigation of an actual HAWC glass fragment obtained from the Karlsruhe vitrification plant (VEK)
2015. Journal of nuclear materials, 460
doi: 10.554/IR/110100079

Zitierung der Originalveröffentlichung:

Dardenne, K.; Gonzalez-Robles, E.; Rothe, J.; Müller, N.; Christill, G.; Lemmer, D.; Praetorius, R.; Kienzler, B.; Metz, V.; Roth, G.; Geckeis, H.
XAS nd XRF investigation of an actual HAWC glass fragment obtained from the Karlsruhe vitrification plant (VEK)
2015. Journal of nuclear materials, 460, 209–215.
doi:10.1016/j.jnucmat.2015.02.021

Lizenzinformationen: CC BY-NC-ND 4.0